Published in "Analytical Chemistry 92(1): 561–566, 2020"
which should be cited to refer to this work.

Resolution Limit of Taylor Dispersion: An Exact Theoretical Study

Patricia Taladriz-Blanco,[†] Barbara Rothen-Rutishauser,[†] Alke Petri-Fink,[†,‡] and Sandor Balog*,[†]

[†]Adolphe Merkle Institute, University of Fribourg, Chemin des Verdiers 4, 1700 Fribourg, Switzerland
[‡]Chemistry Department, University of Fribourg, Chemin du Musée 9, 1700 Fribourg, Switzerland

Supporting Information

ABSTRACT: Taylor dispersion is a microfluidic analytical technique with a high dynamic range and therefore is suited well to measuring the hydrodynamic radius of small molecules, proteins, supramolecular complexes, macromolecules, nanoparticles and their self-assembly. Here we calculate an unaddressed yet fundamental property: the limit of resolution, which is defined as the smallest change in the hydrodynamic radius that Taylor dispersion can resolve accurately and precisely. Using concepts of probability theory and inferential statistics, we present a comprehensive theoretical approach, addressing uniform and polydisperse particle systems, which involve either model-based or numerical analyses. We find a straightforward scaling relationship in which the resolution limit is linearly proportional to the optical-extinction-weighted average hydrodynamic radius of the particle systems.

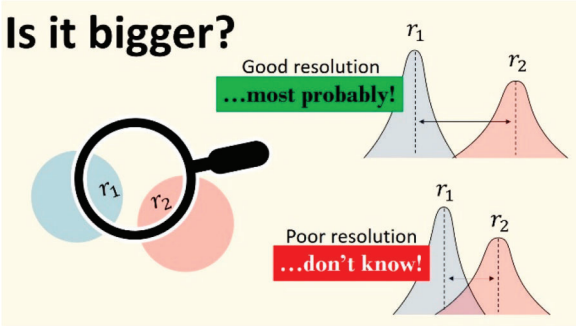

Taylor dispersion, being akin to dynamic light scattering, enables measuring the hydrodynamic radius of particle systems but is less liable to a moderate presence of sample impurities,[1,2] and therefore there is a considerable interest from bionanotechnology, including pharmacology and toxicology in the technique.[3−24]

The question we address in this Letter is straightforward and addresses an elementary analytical property that has never been studied before: What is the resolution limit of Taylor dispersion? By definition, the resolution limit is the smallest change, let it be either increment or decrement in the hydrodynamic radius r, that Taylor dispersion is able to measure accurately and precisely. In other words, it is the smallest δr value where the chance of failing to resolve the difference between r and $r \pm \delta r$ is practically zero. To justify the subject, it is indisputable that a fine limit of resolution is essential to evidence and quantify subtle changes. For instance, characterizing the hydrodynamic radius marks the stages of protein denaturation,[25] polymer degradation,[26] solvent-dependent conformation,[27] and dissolution of ingested nanoparticles.[28] Taylor dispersion is linear and time-invariant,[29] and accordingly, it is possible to resolve the distribution of the hydrodynamic radius of polydisperse and multimodal systems by inverting ("deconvoluting") Gaussian superpositions.[10,15] Accordingly, better measurements pave the way for a deeper understating of, e.g., the interaction of proteins with surfactants[30] and lipids,[31] biological activity of particulate nanomaterials,[32,33] etc., which all arguably result in safer food ingredients, more natural personal hygiene products,[34] and novel therapeutics superior to current standards.[35]

Taylor dispersion combines the phenomenon of optical extinction, translational self-diffusion, and sheer-induced dispersion in a steady Poiseuille flow.[36−38] An initially narrow band of the injected analyte broadens along the capillary upon traveling with the flow, and the extent of band-broadening contains accurate information about the translational self-diffusion coefficient of the dispersed material. The so-called taylorgram is the temporal record of the band broadening, and the concentration is usually measured via UV−vis spectroscopy. If the detector response is linear, and the volume of the injected sample and the volume of detection are both negligibly small compared to the capillary volume, the taylorgram of a uniform material of hydrodynamic radius r dispersed in a cylindrical channel is[36−38]

$$A(t) = A_0 \frac{1}{\sqrt{\pi\kappa t}}\, e^{-(t-t_0)^2/\kappa t} \tag{1}$$

where A_0 is the amplitude of the absorbance, quantified by particle type, particle concentration, and capillary radius Y, $\kappa = r\pi\eta Y^2/(2\, k_B T)$, T is temperature, η is viscosity of the fluid, k_B is the Boltzmann constant, and $t_0 = x/v$ is the so-called residence time defined by the distance between detection and injection points and the mean velocity of the flow (v). The temporal mean and variance of the absorbance profile are $t_0 + \kappa/2$ and $(t_0 + \kappa)\kappa/2$. When the residence time t_0 is much larger than κ, eq 1 is essentially Gaussian, and one can accurately measure the hydrodynamic radius, by determining κ from the absorbance profile

$$r = \frac{2k_B T}{\pi\eta Y^2}\kappa \tag{2}$$

Taylor dispersion is subject to errors that erode the reliability of determining r. Errors are classified as either systematic or random, and the impact of the latter is referred to as precision, which is usually quantified either as standard deviation or relative standard deviation of a set of measurements. Precision may be considered at three levels: repeatability, intermediate precision, and reproducibility. It has been shown recently that the variables in eq 2, the width-parameter κ, temperature T, viscosity η, and capillary radius Y, are directly relevant to the precision of the Taylor dispersion, and the precision may be expressed via the expectable errors of the corresponding variables[39]

$$\Delta r = r\sqrt{\left(\frac{\Delta\kappa}{\kappa}\right)^2 + \left(\frac{\Delta T}{T}\right)^2 + \left(\frac{\Delta\eta}{\eta}\right)^2 + \left(2\frac{\Delta Y}{Y}\right)^2} \tag{3}$$

Here we are building on this result, while considering that the fundamental aspect of experimentation is simple: one performs and analyzes $n = 1,2,3,\ldots n$ measurements independently, under identical conditions, and usually reports the average and standard deviation of the n results. From a statistical point of view, a set of such results is a random sample, with a sample size of n, drawn from the population whose parameters are r and Δr (eqs 2 and 3).[38] The population is the ensemble of the realizable measurement, and owing to random errors, the population is heterogeneous. In other words, if one measures n times, which in technical terms means sampling with replacement, where one draws randomly and independently n elements of the population, one tends to obtain n different results owing to sample-to-sample variations. According to the central limit theorem, the sampling distribution of the mean approximates a normal distribution, regardless of the shape of the distribution describing the population. If r and Δr are the population parameters of a normal distribution, the distribution of the sample mean r_s is practically already normal at small sample sizes ($n < 10$)

$$g\left(r, \frac{\Delta r}{\sqrt{n}}\right) \cong \frac{\sqrt{n}}{\sqrt{2\pi}\,\Delta r}\, e^{-n(r_s - r)^2/2\Delta r^2} \tag{4}$$

with a mean equal to r, and with a standard deviation equal to $\Delta r/\sqrt{n}$. The latter is frequently referred to as the standard error of the mean.

The expectable precision of determining the hydrodynamic radius is therefore $\Delta r/\sqrt{n}$. As a result, the sampling distributions corresponding to two sets of measurements of two hydrodynamic radii that are close to each other may overlap (Figure 1). This may be the case when $r_1 < r_2$ with $r_2/r_1 \cong 1$, i.e., when the difference between r_1 and r_2 is small.

When the overlap is considerable, the chance of evidencing the difference between r_2 and r_1 is low. This is because the chance of ambiguous results increases with the area defined by the overlap, and to be able to quantify the difference between r_2 and r_1, the overlap of the two sampling distributions must be vanishingly small. Otherwise, the chance that the two sample means falling in the area of the overlap becomes high enough. According to eq 4, to decrease the area of the overlap, one must (a) either increase the distance between r_1 and r_2, (b) increase the precision of measuring r_1 and r_2 (i.e., decrease Δr, eq 3), and (c) increase the sample size n (number of measurements). Therefore, the minimum distance (i.e., the difference in size) that can be resolved between r_1 and r_2 is defined by the sample size and the precision attainable in the measurements.

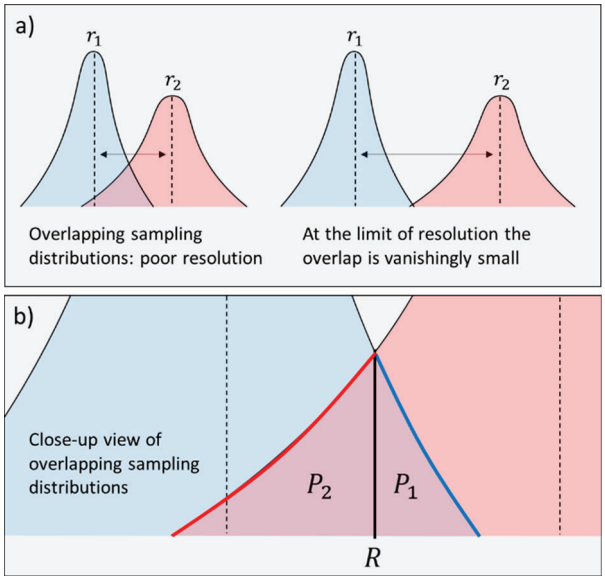

Figure 1. Concept of determining the limit of resolution based on the sampling distribution of the mean (eq 4). The sampling distributions corresponding to two sets of measurements of two hydrodynamic radii r_1 and r_2 may overlap when r_1 and r_2 are close enough to one another. If the overlap is considerable, the chance of evidencing the difference between the two is low (a). This is significant, because the chance of ambiguous results, where either $R < r_s(1)$ or $r_s(2) < R$ or $r_s(2) < R < r_s(1)$ increases with the area of the overlap (b). To be able to discern the difference between r_1 and r_2 with a high certainty, the overlap of the two sampling distributions must be vanishingly small.

This qualitative picture is quantified next, and we show that the overlap has a clear probabilistic meaning, which is then applied to give a quantitative and clearly defined answer to the limit of resolution of Taylor dispersion. As illustrated in Figure 1b, the area of the overlap is the sum of two components: $P_1 + P_2$ where

$$P_1 = \int_R^{\infty} g\left(r_1, \frac{\Delta r_1}{\sqrt{n_1}}\right) dr = \frac{1}{2} - \frac{1}{2}\,\mathrm{erf}\left(\frac{\sqrt{n_1}(R - r_1)}{\sqrt{2}\,\Delta r_1}\right) \tag{5}$$

$$P_2 = \int_{-\infty}^{R} g\left(r_2, \frac{\Delta r_2}{\sqrt{n_2}}\right) dr = \frac{1}{2} + \frac{1}{2}\,\mathrm{erf}\left(\frac{\sqrt{n_2}(R - r_2)}{\sqrt{2}\,\Delta r_2}\right) \tag{6}$$

Each component represents a cumulative probability: P_1 is the cumulative probability that the mean value of the n_1 measurements of the hydrodynamic radius r_1 falls over the intersection point R, and P_2 is the cumulative probability that the mean value of the n_2 measurements of the hydrodynamic radius r_2 falls below the intersection point R. Therefore, the area of the overlap quantifies the probability $P = P_1 + P_2$ that the mean of either or both of the measurements falls on a "wrong" interval of the sampling distributions. Naturally, if this probability is small, the chance of evidencing the difference between r_1 and r_2 is high.

The intersection point $r_1 < R < r_2$ can be found by solving the equation

$$g\left(r_1, \frac{\Delta r_1}{\sqrt{n_1}}\right) = g\left(r_2, \frac{\Delta r_2}{\sqrt{n_2}}\right) \tag{7}$$

By following some basic algebraic steps, a rearranged form gives a simple quadratic equation

$$\frac{n_2(x - r_2)^2}{2\Delta r_2^{\,2}} - \frac{n_1(x - r_1)^2}{2\Delta r_1^{\,2}} = Z_1 \tag{8}$$

where $Z_1 = \ln\left(\frac{\Delta r_1\sqrt{n_2}}{\Delta r_2\sqrt{n_1}}\right)$, and the nontrivial solution provides two roots

$$R = \frac{n_2 r_2 \Delta r_1^{\,2} \pm \Delta r_2(\Delta r_1\sqrt{Z_2} \mp n_1 r_1 \Delta r_2)}{n_2 \Delta r_1^{\,2} - n_1 \Delta r_2^{\,2}} \tag{9}$$

where $Z_2 = n_2(n_1(r_1 - r_2)^2 + 2Z_1\Delta r_1^{\,2}) - 2Z_1 n_1 \Delta r_2^{\,2}$. The solution we need is the one that is larger than r_1 but smaller than r_2, i.e., $r_1 < R < r_2$.

While eq 9 is a general solution, it may be simplified considerably by considering a special case. First, the sample size is commonly kept symmetric in experimental practice, i.e., $n_1 = n_2$, and second, according to eq 3, near to the limit of resolution $\Delta r_2 \cong \Delta r_1$ because $r_2/r_1 \cong 1$. By considering these two aspects, we obtain that $R \cong (r_1 + r_2)/2$, and inserting them into eqs 5 and 6, the area of the overlap is expressed in a straightforward manner

$$P = P_1 + P_2 \cong 1 - \mathrm{erf}\left(\frac{\sqrt{n}\,(r_2 - r_1)}{\sqrt{8}\,\Delta r}\right) \tag{10}$$

where $n = n_1 = n_2$ is the number of measurements and $\Delta r = \Delta r_1 \cong \Delta r_2$ is the precision of the measurements determining r_2 and r_1. The function $f(x) = 1 - \mathrm{erf}(x)$ is shown in Figure 2.

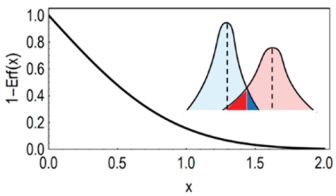

Figure 2. $f(x) = 1 - \mathrm{erf}(x)$ function describing eq 10. When $f(x)$ is vanishingly small, the probability of obtaining ambiguous results P is also vanishingly small, i.e., the difference between r_1 and r_2 is surely expected to be evidenced.

As can be seen, $f(x)$ is a monotone decreasing function that asymptotically approaches zero. In other words, there is a definite relationship between x and P: if x keeps increasing, P keeps decreasing, and the probability of obtaining ambiguous results eventually becomes vanishingly small. The inverse of this relationship is also true: when P is small, x and thus $r_2 - r_1$ must be also small. Accordingly, the smaller P, the higher the probability that the difference between r_2 and r_1 is discerned and quantified from the recorded taylorgrams.

Therefore, based on eq 10, we can quantify the limit of resolution with a probabilistic exactness: Let δr be the smallest value where the odds in favor of resolving r and $r + \delta r$ are not smaller than a million to one, that is, the probability of obtaining ambiguous results is 10^{-6}

$$\delta r = \varphi\frac{\Delta r}{\sqrt{n}} \tag{11}$$

where $\varphi \cong 9.78$ when $P = 10^{-6}$. If one is less cautious and willing to accept a higher risk of obtaining ambiguous measurements, the value of P may be increased, and accordingly δr may be smaller. For example, $\varphi \cong 6.58$ when $P = 10^{-3}$.

It is important to emphasize that according to eqs 5−11, the limit of resolution is not a universal but a rather supple parameter. It is in fact limited by the design of the experiments and the quality of the related analysis, because it is a function of (1) the probability of obtaining ambiguous results, (2) the number of measurements we are willing or able to collect and analyze, and (3) the precision one is willing (and able) to achieve in these measurements. For example, it matters whether the width parameter κ of the taylorgram is estimated by a nonlinear regression of eq 1 or by a direct numerical integration of the taylorgram itself, for the attainable precision of $\Delta\kappa$ will not be identical.[16,39] Furthermore, given that Δr is a function of r, δr becomes also a function of r, and it is easy to show via eq 3 that by using a typical Taylor dispersion system, including typical instrument and experimental parameters, the limit of resolution is proportional the hydrodynamic radius: $\Delta r \propto r$.

We showed previously that by using unconstrained nonlinear least-squares fit to estimate the width parameter of a taylorgram of uniform particles, $\Delta\kappa$ can be expressed as a function of four parameters: $\Delta\kappa = z\kappa^{B+1}t_0^{\,C}\tau^D\mathrm{SN}^E$, where $z = 2.42$ is a dimensionless constant, κ the value defined by the uniform hydrodynamic radius of the particles, t_0 residence time, τ the temporal resolution of the taylorgram, and SN the signal-to-noise ratio. The exponents are $= -0.24$, $C = -0.26$, $D = 0.5$, and $E = -1$.[16]

Nonuniform particle systems, including polydispersity and multimodality, are however frequent, and their taylorgrams are analyzed in terms of temporal moments such as mean and variance to determine the optical-extinction-weighted average radius.[6,12,20,23,40,41] This approach involves numerical integration, and noise affects the attainable precision differently than it affects model-based nonlinear regression.[39] The residence time and width parameter are determined through the temporal mean (M) and temporal variance (V), and it was shown elsewhere[20,23] that in the case of Rayleigh particle systems, where optical absorption and scattering are power functions of the particle radius (i.e., optical absorption coefficient at a given wavelength of a particle is proportional to its volume), the apparent hydrodynamic radius determined by Taylor dispersion is $r_{\mathrm{poly}} = \widetilde{r^{m+1}}/\widetilde{r^m}$, where $\widetilde{r^m}$ is the mth raw moment of the size distribution of the particle system: $\widetilde{r^m} \equiv \int_0^\infty P(r)\cdot r^m\,\mathrm{d}r$. Accordingly, for particles system whose optical extinction is dominated by, e.g., absorption: $r_{\mathrm{poly}} = \widetilde{r^4}/\widetilde{r^3}$. Thus, in the case of size polydispersity: $M \cong t_0 + 1/2\,\kappa_{\mathrm{poly}}$ and $V \cong 1/2\,\kappa_{\mathrm{poly}} \cdot (t_0 + \kappa_{\mathrm{poly}})$, where the apparent width parameter is $\kappa_{\mathrm{poly}} = r_{\mathrm{poly}}\pi\eta Y^2/(2\,k_{\mathrm{B}}T)$. When $t_0 \gg \kappa_{\mathrm{poly}}$, $M \cong t_0$ and $V \cong t_0 \cdot \kappa_{\mathrm{poly}}/2$, and thus

$$\kappa_{\mathrm{poly}} \cong \frac{2V}{M} \tag{12}$$

and the corresponding relative uncertainty is

$$\left(\frac{\Delta\kappa_{\text{poly}}}{\kappa_{\text{poly}}}\right)^2 \cong \frac{\sigma_{\text{M}}{}^2}{M^2} + \frac{\sigma_{\text{V}}{}^2}{V^2} \tag{13}$$

where $\sigma_{\text{M}}{}^2$ and $\sigma_{\text{V}}{}^2$ describe the uncertainty, owing to the presence of noise, of determining the temporal mean and temporal variance of the taylogram via numerical integration. To calculate $\sigma_{\text{M}}{}^2$ and $\sigma_{\text{V}}{}^2$ is not trivial.[39] Briefly, when the signal-to-noise ratio is not too low (i.e., the peak of the taylorgram is clearly recognizable: SN > 2), the experimentally recorded taylorgram may be decomposed into two terms, $A_\epsilon = A + \epsilon$, where ϵ represents additive noise. The origin of ϵ is the shot noise,[23] and its probability density function $p(\epsilon)$ is practically Gaussian. It is easy to show that $p(\epsilon)$ is practically stationary in time when the peak absorbance is not too high (i.e., $A(t_0) < 0.1$), which means that the variance of $p(\epsilon)$ is practically constant along the taylorgram. The value of ϵ varies randomly along the taylorgram with a zero mean $\overline{\epsilon} = 0$ and variance $\overline{\epsilon^2} - \overline{\epsilon}^2 = \overline{\epsilon^2}$. The noise in a taylorgram is uncorrelated, that is $\overline{\epsilon_i\epsilon_j} = \overline{\epsilon^2}\delta_{ij}$, where δ_{ij} is the Kronecker delta. The overline denotes ensemble average:

$$\overline{\epsilon} = \int_{-\infty}^{\infty} \epsilon p(\epsilon)\, \mathrm{d}\epsilon \tag{14}$$

and

$$\overline{\epsilon^2} = \int_{-\infty}^{\infty} \epsilon^2 p(\epsilon)\, \mathrm{d}\epsilon \tag{15}$$

Following the definition of the signal-to noise ratio of a taylorgram,[23] it is not difficult to show that $\sqrt{\overline{\epsilon^2}} \cong A(t_0)/\text{SN}$

The temporal moments of a taylorgram calculated as a normalized temporal average on the closed interval capped by t_a and t_b, and is defined as

$$\langle t^w A_\epsilon(t)\rangle = \frac{\int_{t_a}^{t_b} t^w A_\epsilon(t)\, \mathrm{d}t}{\int_{t_a}^{t_b} A_\epsilon(t)\, \mathrm{d}t} \tag{16}$$

where $w = 1$ or 2, t_a and t_b enclose the peak of the taylorgram and are chosen symmetrically around the center of the peak. In experimental practice, a taylorgram is recorded with discrete time points, and thus the integration of such real-valued function becomes a summation (Riemann sum), e.g.:

$$\int_{t_a}^{t_b} A_\epsilon(t)\, \mathrm{d}t \cong \tau \sum_{i=1}^{k} A_\epsilon(t_i) \tag{17}$$

where τ is the temporal resolution, i.e., $t_1 = t_a$, $t_2 = t_1 + \tau$, $t_j = t_1 + (j - 1)\tau$, and $t_b = t_1 + k\tau$, and $k \gg 1$. Accordingly,

$$M \cong \frac{\tau \sum_{i=1}^{k} t_i A_\epsilon(t_i)}{\tau \sum_{i=1}^{n} A_\epsilon(t_i)} \tag{18}$$

and

$$V \cong \frac{\tau \sum_{i=1}^{k} t_i{}^2 A_\epsilon(t_i)}{\tau \sum_{i=1}^{k} A_\epsilon(t_i)} - M^2 \tag{19}$$

In the absence of noise, the precision and accuracy are perfect, and determining the true values of M, V and κ_{poly} is completely assured. Given the noise, however, both M and V may vary from taylorgram to taylorgram, and accordingly, there is uncertainty, and thus $\sigma_{\text{M}}{}^2 > 0$, $\sigma_{\text{V}}{}^2 > 0$ and $\Delta\kappa_{\text{poly}} > 0$. Their expected values are calculated via ensemble averaging over the noise distribution

$$\overline{M} = \int_{-\infty}^{\infty} M p(\epsilon)\, \mathrm{d}\epsilon \tag{20}$$

$$\overline{V} = \int_{-\infty}^{\infty} V p(\epsilon)\, \mathrm{d}\epsilon \tag{21}$$

$$\sigma_{\text{M}}{}^2 = \overline{M^2} - \overline{M}^2 = \int_{-\infty}^{\infty} M^2 p(\epsilon)\, \mathrm{d}\epsilon - \overline{M}^2 \tag{22}$$

$$\sigma_{\text{V}}{}^2 = \overline{V^2} - \overline{V}^2 = \int_{-\infty}^{\infty} V^2 p(\epsilon)\, \mathrm{d}\epsilon - \overline{V}^2 \tag{23}$$

We could not evaluate these equations, most likely owing to singularities in these improper integrals and thus cannot present general analytical forms. Nonetheless, we found excellent approximative solutions when considering not too high noise levels, i.e., where the peak of the taylorgram is clearly recognizable, or in other words, the signal-to-noise ratio is not vanishing. First, let us define three new variables: $\alpha = \tau \sum_{i=1}^{k} t_i A_\epsilon(t_i)$, $\beta = \tau \sum_{i=1}^{k} t_i{}^2 A_\epsilon(t_i)$, and $\gamma = \tau \sum_{i=1}^{k} A_\epsilon(t_i)$. Consequently, $M = \alpha/\gamma$ and $V = \beta/\gamma - (\alpha/\gamma)^2$. α, β, and γ are correlated random variables, and the uncertainties in M and V may be expressed as[42]

$$\sigma_{\text{M}}{}^2 \cong \left(\frac{\partial M}{\partial \alpha}\right)^2 \sigma_\alpha{}^2 + \left(\frac{\partial M}{\partial \gamma}\right)^2 \sigma_\gamma{}^2 + 2\,\text{Cov}(\alpha, \gamma) \tag{24}$$

and

$$\sigma_{\text{V}}{}^2 \cong \left(\frac{\partial M}{\partial \alpha}\right)^2 \sigma_\alpha{}^2 + \left(\frac{\partial M}{\partial \beta}\right)^2 \sigma_\beta{}^2 + \left(\frac{\partial M}{\partial \gamma}\right)^2 \sigma_\gamma{}^2 + 2\,\text{Cov}(\alpha, \gamma) + 2\,\text{Cov}(\alpha, \beta) + 2\,\text{Cov}(\beta, \gamma) \tag{25}$$

The partial derivatives are to be evaluated at $\overline{\alpha}$, $\overline{\beta}$ and $\overline{\gamma}$. Equations 24 and 25 can be evaluated analytically, and therefore, we are still able to describe the uncertainty of numerical integration. For example, $\overline{\gamma} = \int_{-\infty}^{\infty} \gamma p(\epsilon)\, \mathrm{d}\epsilon = \tau \int_{-\infty}^{\infty} \sum_{i=1}^{k} A(t_i) p(\epsilon)\, \mathrm{d}\epsilon + \tau \int_{-\infty}^{\infty} \sum_{i=1}^{k} \epsilon(t_i) p(\epsilon)\, \mathrm{d}\epsilon$. The first term is the area under the taylorgram, and the second term vanishes because the mean of the additive noise is zero. We could evaluate similarly the other terms, and the results are

$$\overline{\alpha} = \tau \sum_{i=1}^{k} t_i A(t_i) \tag{26}$$

$$\overline{\beta} = \tau \sum_{i=1}^{k} t_i{}^2 A(t_i) \tag{27}$$

$$\overline{\gamma} = \tau \sum_{i=1}^{k} A(t_i) \tag{28}$$

$$\sigma_\alpha{}^2 = \tau^2 \sigma_{\text{N}}{}^2 \sum_{i=1}^{k} t_i{}^2 \tag{29}$$

$$\sigma_\beta{}^2 = \tau^2 \sigma_{\text{N}}{}^2 \sum_{i=1}^{k} t_i{}^4 \tag{30}$$

$$\sigma_\gamma^2 = \tau^2 \sigma_N^2 k \tag{31}$$

$$\mathrm{Cov}(\alpha, \gamma) = \tau^2 \sigma_N^2 \sum_{i=1}^{k} t_i \tag{32}$$

$$\mathrm{Cov}(\alpha, \beta) = \tau^2 \sigma_N^2 \sum_{i=1}^{k} t_i^3 \tag{33}$$

$$\mathrm{Cov}(\beta, \gamma) = \tau^2 \sigma_N^2 \sum_{i=1}^{k} t_i^2 \tag{34}$$

where $\sigma_N^2 = \overline{\epsilon^2} \cong (A(t_0)/\mathrm{SN})^2$, $\overline{M} \cong \overline{\alpha}/\overline{\gamma}$ and $\overline{V} \cong \overline{\beta}/\overline{\gamma} - (\overline{\alpha}/\overline{\gamma})^2$. Accordingly, the resolution in determining the hydrodynamic radius via numerical integration can be evaluated via eqs 12−35. One frequently combines the analyses of two detection windows to determine the hydrodynamic radius[11,12]

$$\kappa_{\mathrm{poly}} = 2\frac{V(t_2) - V(t_1)}{M(t_2) - M(t_1)} \tag{35}$$

The related uncertainty is

$$\left(\frac{\Delta\kappa_{\mathrm{poly}}}{\kappa_{\mathrm{poly}}}\right)^2 \cong \frac{\sigma_M^2(t_2)}{(M(t_2) - M(t_1))^2} + \frac{\sigma_M^2(t_1)}{(M(t_2) - M(t_1))^2} + \frac{\sigma_V^2(t_2)}{(V(t_2) - V(t_1))^2} + \frac{\sigma_V^2(t_1)}{(V(t_2) - V(t_1))^2} \tag{36}$$

When it comes to numerical integration, the uncertainty is increasing with the level of noise (σ_N) and with the length of the integration interval ($t_b - t_a$, eq 16). This is because in eqs 29−34

$$\sum_{i=1}^{k} t_i = \frac{1}{2}(t_a + t_b) + \frac{1}{2\tau}(t_b^2 - t_a^2) \tag{37}$$

$$\sum_{i=1}^{k} t_i^2 = \frac{1}{2}(t_a^2 + t_b^2) + \frac{\tau}{6}(t_b - t_a) + \frac{1}{3\tau}(t_b^3 - t_a^3) \tag{38}$$

$$\sum_{i=1}^{k} t_i^3 = \frac{1}{2}(t_a^3 + t_b^3) + \frac{\tau}{4}(t_b^2 - t_a^2) + \frac{1}{4\tau}(t_b^4 - t_a^4) \tag{39}$$

$$\sum_{i=1}^{k} t_i^4 = \frac{1}{2}(t_a^4 + t_b^4) + \frac{\tau^3}{30}(t_a - t_b) + \frac{\tau}{3}(t_b^3 - t_a^3) + \frac{1}{5\tau}(t_b^5 - t_a^5) \tag{40}$$

Equations 37−40 mean that the uncertainty of determining the width and center of a taylorgram increases with the residence time ($t_0 \cong (t_a + t_b)/2$) and with the length of the integration intervals ($t_b - t_a$). It is worth pointing out that the uncertainty resulting from numerical integration is always inferior to that of resulting from suitable model fitting.

To summarize, the hydrodynamic radius is a fundamental physical property, for it can indicate the onset of even minute changes in the properties of a particle dispersion, let it be natural or engineered of origin. By using concepts of probability theory and inferential statistics, we showed here that the limit of resolution of Taylor dispersion is inherently defined by the precision attained in the given sets of measurements, and the limit of resolution ultimately scales with $r/\sqrt{n}$, where n is the number of measurements used to determine the mean value.

To demonstrate some aspects of our findings, we present two complete studies in the Supporting Information. The first one is a brief theoretical study that addresses a special case: uniform particles and model fitting (The ultimate resolution limit of Taylor dispersion for uniform particle systems, Figure SI 1). Our goal was to point out that the resolution limit of optimal "noise-limited" Taylor dispersion experiments may be outstanding, which offers a performance competitive to well-established and widely used techniques, such as dynamic light scattering, fluorescence correlation spectroscopy, particle tracking analysis, and small-angle X-ray and neutron scattering. The second one is an experimental study that addresses a highly polydisperse particle system (The stability and hydrodynamic radius of citrate-capped silver nanoparticles in water, Figures SI 2−8). Our goal was to demonstrate how the theory developed in this Letter may be used to design, analyze, and interpret fully realistic scenarios of Taylor dispersion experiments.

■ ASSOCIATED CONTENT

Supporting Information

The Supporting Information is available free of charge at https://pubs.acs.org/doi/10.1021/acs.analchem.9b03837.

Two complete studies: ultimate resolution limit of Taylor dispersion for uniform particle systems and stability and hydrodynamic radius of citrate-capped silver nanoparticles in water (PDF)

■ AUTHOR INFORMATION

Corresponding Author

*E-mail: sandor.balog@unifr.ch.

ORCID

Patricia Taladriz-Blanco: 0000-0002-2469-9704

Alke Petri-Fink: 0000-0003-3952-7849

Sandor Balog: 0000-0002-4847-9845

Author Contributions

S.B. conceived the idea, developed the theoretical description, and wrote the manuscript through contributions of the coauthors. S.B. and P.T.-B. designed the experimental study. P.T.-B. synthesized the particles, performed the UV−vis, the TEM, and the Taylor dispersion experiments. S.B. and P.T.-B. analyzed the experimental evidence. A.P.-F. and B.R.-R. supervised P.T.-B.

Notes

The authors declare no competing financial interest.

■ ACKNOWLEDGMENTS

The authors are grateful for the financial support of the Adolphe Merkle Foundation and the University of Fribourg. This work also benefitted from support (<50%) of the Swiss National Science Foundation through the National Center of Competence in Research Bio-Inspired Materials.

■ REFERENCES

(1) Hawe, A.; Hulse, W. L.; Jiskoot, W.; Forbes, R. T. *Pharm. Res.* **2011**, *28*, 2302−2310.

(2) Urban, D. A.; Milosevic, A. M.; Bossert, D.; Crippa, F.; Moore, T. L.; Geers, C.; Balog, S.; Rothen-Rutishauser, B.; Petri-Fink, A. *Colloid and Interface Science Communications* **2018**, *22*, 29–33.
(3) Bello, M. S.; Rezzonico, R.; Righetti, P. G. *Science* **1994**, *266*, 773–776.
(4) Belongia, B. M.; Baygents, J. C. *J. Colloid Interface Sci.* **1997**, *195*, 19–31.
(5) Wuelfing, W. P.; Templeton, A. C.; Hicks, J. F.; Murray, R. W. *Anal. Chem.* **1999**, *71*, 4069–4074.
(6) Cottet, H.; Biron, J.-P.; Martin, M. *Anal. Chem.* **2007**, *79*, 9066–9073.
(7) d'Orlyé, F.; Varenne, A.; Gareil, P. *Journal of Chromatography A* **2008**, *1204*, 226–232.
(8) Le Saux, T.; Cottet, H. *Anal. Chem.* **2008**, *80*, 1829–1832.
(9) Medina, C.; Santos-Martinez, M. J.; Radomski, A.; Corrigan, O. I.; Radomski, M. W. *Br. J. Pharmacol.* **2007**, *150*, 552–558.
(10) Cottet, H.; Biron, J.-P.; Cipelletti, L.; Matmour, R.; Martin, M. *Anal. Chem.* **2010**, *82*, 1793–1802.
(11) Hulse, W.; Forbes, R. *Int. J. Pharm.* **2011**, *416*, 394–397.
(12) Chamieh, J.; Oukacine, F.; Cottet, H. *J. Chromatogr A* **2012**, *1235*, 174–177.
(13) Cipelletti, L.; Biron, J.-P.; Martin, M.; Cottet, H. *Anal. Chem.* **2014**, *86*, 6471–6478.
(14) Jensen, S. S.; Jensen, H.; Cornett, C.; Møller, E. H.; Østergaard, J. *J. Pharm. Biomed. Anal.* **2014**, *92*, 203–210.
(15) Cipelletti, L.; Biron, J.-P.; Martin, M.; Cottet, H. *Anal. Chem.* **2015**, *87*, 8489–8496.
(16) Lavoisier, A.; Schlaeppi, J.-M. *mAbs* **2015**, *7*, 77–83.
(17) Oukacine, F.; Morel, A.; Desvignes, I.; Cottet, H. *J. Chromatogr A* **2015**, *1426*, 220–225.
(18) Pyell, U.; Jalil, A. H.; Urban, D. A.; Pfeiffer, C.; Pelaz, B.; Parak, W. J. *J. Colloid Interface Sci.* **2015**, *457*, 131–140.
(19) Høgstedt, U. B.; Schwach, G.; van de Weert, M.; Østergaard, J. *Eur. J. Pharm. Sci.* **2016**, *93*, 21–28.
(20) Balog, S.; Urban, D. A.; Milosevic, A. M.; Crippa, F.; Rothen-Rutishauser, B.; Petri-Fink, A. *J. Nanopart. Res.* **2017**, *19*, 287.
(21) Fichtner, A.; Jalil, A.; Pyell, U. *Langmuir* **2017**, *33*, 2325–2339.
(22) Zaman, H.; Bright, A. G.; Adams, K.; Goodall, D. M.; Forbes, R. T. *Int. J. Pharm.* **2017**, *522*, 98–109.
(23) Balog, S. *Anal. Chem.* **2018**, *90*, 4258–4262.
(24) Oukacine, F.; Gèze, A.; Choisnard, L.; Putaux, J.-L.; Stahl, J.-P.; Peyrin, E. *Anal. Chem.* **2018**, *90*, 2493–2500.
(25) Jelińska, A.; Zagożdżon, A.; Górecki, M.; Wisniewska, A.; Frelek, J.; Holyst, R. *PLoS One* **2017**, *12*, No. e0175838.
(26) Chamieh, J.; Biron, J. P.; Cipelletti, L.; Cottet, H. *Biomacromolecules* **2015**, *16*, 3945–3951.
(27) Jin, X.; Leclercq, L.; Sisavath, N.; Cottet, H. *Macromolecules* **2014**, *47*, 5320–5327.
(28) Bove, P.; Malvindi, M. A.; Kote, S. S.; Bertorelli, R.; Summa, M.; Sabella, S. *Nanoscale* **2017**, *9*, 6315–6326.
(29) Lemal, P.; Petri-Fink, A.; Balog, S. *Anal. Chem.* **2019**, *91*, 1217–1221.
(30) Otzen, D. *Biochim. Biophys. Acta, Proteins Proteomics* **2011**, *1814*, 562–591.
(31) Serrano, A. G.; Pérez-Gil, J. *Chem. Phys. Lipids* **2006**, *141*, 105–118.
(32) Shaw, S. Y.; Westly, E. C.; Pittet, M. J.; Subramanian, A.; Schreiber, S. L.; Weissleder, R. *Proc. Natl. Acad. Sci. U. S. A.* **2008**, *105*, 7387.
(33) Epa, V. C.; Burden, F. R.; Tassa, C.; Weissleder, R.; Shaw, S.; Winkler, D. A. *Nano Lett.* **2012**, *12*, 5808–5812.
(34) Buzea, C.; Pacheco, I. I.; Robbie, K. *Biointerphases* **2007**, *2*, MR17–MR71.
(35) Salata, O. V. *J. Nanobiotechnol.* **2004**, *2*, 3.
(36) Taylor, G. I. *Proc. R. Soc. Lond. A* **1953**, *219*, 186–203.
(37) Taylor, G. I. *Proc. R. Soc. Lond. A* **1954**, *225*, 473–477.
(38) Aris, R. *Proc. R. Soc. Lond. A* **1956**, *235*, 67–77.
(39) Taladriz-Blanco, P.; Rothen-Rutishauser, B.; Petri-Fink, A.; Balog, S. *Anal. Chem.* **2019**, *91*, 9946–9951.
(40) Cottet, H.; Martin, M.; Papillaud, A.; Souaïd, E.; Collet, H.; Commeyras, A. *Biomacromolecules* **2007**, *8*, 3235–3243.
(41) Chamieh, J.; Cottet, H. *Journal of Chromatography A* **2012**, *1241*, 123–127.
(42) De Bièvre, P. *Accredit. Qual. Assur.* **2012**, *17*, 231–232.